VIP Heterogeneous Catalysis

DOI: 10.1002/anie.201203755

A Highly Reactive and Sinter-Resistant Catalytic System Based on Platinum Nanoparticles Embedded in the Inner Surfaces of CeO_2 Hollow Fibers**

*Kyunghwan Yoon, Yong Yang, Ping Lu, Dehui Wan, Hsin-Chieh Peng, Kimber Stamm Masias, Paul T. Fanson, Charles T. Campbell, and Younan Xia**

The catalytic properties of a supported system are strongly dependent on the types of metal and supporting material involved.[1–4] Platinum nanoparticles (NPs) supported on ceria (CeO_2) have shown higher catalytic activities for a wide variety of reactions, including water-gas shift,[5,6] CO oxidation,[7] and hydrogenation[8,9] when compared to those supported on other oxides. Therefore, CeO_2 has been widely employed as a support for manufacturing automotive catalysts because of its peerless oxygen storing/releasing capabilities as well as its superior ability to stabilize noble metals.[10,11] In particular, Pt/CeO_2 catalysts are known to exhibit strong metal–support interaction effects with a potential to enhance the catalytic activities for reactions involving rapid oxygen and/or electron transfer between the metal and the support.[12–15] Although there are many benefits in utilizing the Pt/CeO_2 system in real-world catalytic applications, great challenges, such as low thermal stability and loss of catalytic activity owing to sintering, still need to be addressed. In catalysts for automotive exhaust treatment, these problems are partially mitigated by combining CeO_2 with ZrO_2 in a solid solution, but precious metal sintering remains a primary deterioration mechanism.

The use of nanostructured composite materials is one strategy to address the sintering issue. Yan and co-workers recently synthesized CeO_2 nanoparticles covered with Pt NPs and then SiO_2 shells to protect the Pt NPs from aggregation during calcination,[16] but their approach required multiple steps to generate the SiO_2 shells and then dissolve them. As a major drawback, the Pt/CeO_2 nanocomposites could only withstand calcination up to 450 °C after the removal of the SiO_2 shells. Tsang and co-workers demonstrated the synthesis of a Pt/CeO_2 core–shell NPs by a modified microemulsion method.[17,18] The resultant catalyst showed significantly improved catalytic activity and selectivity in water-gas shift over methanation by controlling the thickness of the CeO_2 protective layer. However, the Pt/CeO_2 core–shell NPs exhibited considerable aggregation in the reaction medium, which may negatively impact their catalytic activity in a practical application.

Herein, we report a simple, template-based procedure for the fabrication of CeO_2 hollow fibers with Pt NPs embedded in the inner surfaces (Figure 1). The first step involved the generation of polystyrene (PS) fibers by electrospinning, followed by plasma treatment to render their surfaces hydrophilic for the deposition of Pt NPs. The deposited Pt NPs then served as nucleation sites to initiate the growth of a uniform sheath of CeO_2 on the surface of each PS fiber. After the removal of PS fibers by calcination in air at 400 °C, we obtained CeO_2 hollow fibers with inner surfaces that were embedded with Pt NPs. In addition to a porous wall, the hollow fiber also had open ends to ensure high permeation and mass transfer rates for species involved in a catalytic reaction. The turnover frequency (TOF) of this new catalytic system for CO oxidation was found to be 2–3 orders of magnitude higher than those of other systems. Thanks to an effective metal–support contact, it was also thermally stable against sintering up to 700 °C.

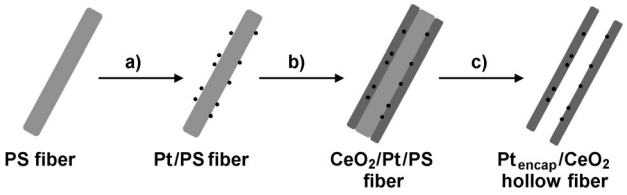

Figure 1. The three-step procedure developed herein for the preparation of Pt_{encap}/CeO_2 hollow fibers with open ends. a) Deposition of Pt NPs; b) coating of CeO_2 sheath; c) removal of PS fiber at 400 °C. Pt_{encap}/CeO_2 designates a CeO_2-supported Pt catalyst in which the Pt NPs are almost completely encapsulated by CeO_2.

[*] Dr. K. Yoon, Dr. P. Lu,[+] Dr. D. Wan,[+] H. Peng,[+] Prof. Y. Xia[+]
Department of Biomedical Engineering
Washington University in St. Louis
St. Louis, MO 63130 (USA)
E-mail: younan.xia@bme.gatech.edu
Dr. Y. Yang, Prof. C. T. Campbell
Department of Chemistry, University of Washington
Seattle, WA 98195 (USA)
Dr. K. Stamm Masias, Dr. P. T. Fanson
Toyota Motor Engineering and Manufacturing North America, Inc.
Ann Arbor, MI 48105 (USA)
[+] Current address: The Wallace H. Coulter Department of Biomedical Engineering and School of Chemistry & Biochemistry
Georgia Institute of Technology, Atlanta, GA 30332 (USA)

[**] This work was supported by the Toyota Motor Engineering and Manufacturing North America, Inc. A portion of the research was performed using UMSL, a national scientific user facility sponsored by the Department of Energy's Office of Biological and Environmental Research and located at Pacific Northwest National Laboratory.

Supporting information for this article is available on the WWW under http://dx.doi.org/10.1002/anie.201203755.

The nonwoven mat of PS fibers was prepared by electrospinning a 20 wt% solution of PS in a mixture of tetrahydrofuran (THF) and dimethylformamide (DMF) at a mass ratio of 1:1. The average diameter of the as-spun PS fibers was 1.16 ± 0.22 μm (Supporting Information, Figure S1a). The Pt NPs stabilized by poly(vinyl pyrrolidinone) (PVP) were prepared using a method based on polyol reduction.[19] The as-synthesized Pt NPs were uniform in size (Figure S1b), with an average diameter of 3.5 nm (Figure S1c). The surface of a plasma-treated PS fiber could be easily coated with the Pt NPs by immersing the fiber mat in a suspension of Pt NPs in ethanol, followed by washing to remove the loosely bound NPs and drying in air (Figure S1d).

The PS fiber decorated with Pt NPs was then employed as a substrate for the in situ growth of a CeO_2 sheath by a process involving reaction of cerium(III) acetate with 6-aminocaproic acid (6ACA) in an aqueous medium in air.[20] As shown in Figure 2a, the CeO_2 coating was deposited uniformly on the surface of each Pt/PS fiber and no interfiber connection was observed. The average diameter of the CeO_2/Pt/PS fibers increased to 1.37 ± 0.30 μm. From the SEM data, the thickness of the CeO_2 sheath was estimated to be about 100 nm in thickness. Based on an XRD pattern (Supporting Information, Figure S2a), the as-deposited CeO_2 coating was crystallized in a cubic fluorite structure ($Fm3m$, $a = 5.411$ Å, JCPDS Card No. 34-0394). It is remarkable that a complete sheath made of crystalline CeO_2 nanoparticles could be formed on the PS fiber under relatively mild reaction conditions (60 °C for 2 h). In this case, the Pt NPs played an important role in the nucleation and growth of CeO_2 nanocrystals in the presence of 6ACA. Because the PVP-stabilized Pt NPs were negatively charged with a zeta potential of −0.83 mV under a slightly basic pH (7.5), the Ce^{3+} cations could easily adsorb onto the Pt NPs to facilitate the nucleation and growth of CeO_2 nanocrystals. Although the details for CeO_2 growth still need to be fully investigated, our TEM observations did provide some evidence to support this proposed mechanism. The organic components in the as-prepared CeO_2/Pt/PS structures, including PS, PVP, and 6ACA, could be removed by calcination in air at an elevated temperature to generate CeO_2 hollow fibers with Pt NPs embedded in the inner surfaces. The SEM image in Figure 2b and the TEM image in the inset clearly show a hollow structure for the CeO_2 fibers. The loading of Pt in the as-prepared Pt_{encap}/CeO_2 hollow fibers was about 0.98%, as determined by inductively coupled plasma mass spectrometry (ICP-MS).

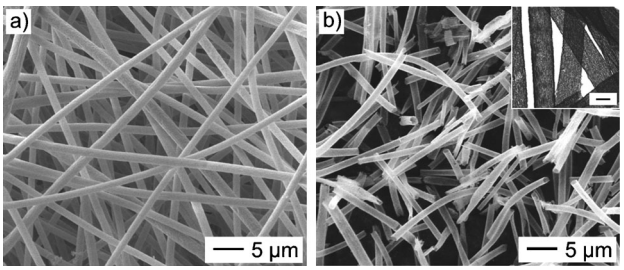

Figure 2. SEM images of PS fibers with surfaces that have been coated with Pt NPs and then CeO_2 sheaths a) before and b) after calcination in air at 400 °C for 2 h. (Inset: TEM image confirming the hollow structure; scale bar: 1 μm).

Figure 3 shows TEM images of the Pt_{encap}/CeO_2 hollow fibers after they had been further treated at different temperatures in air for 2 h. The products obtained at 400 and 800 °C still maintained a tubular structure without being collapsed, demonstrating a rather good thermal stability for the relatively thin CeO_2 sheath. Furthermore, the Pt NPs were effectively prevented from sintering up to 700 °C as a result of the CeO_2 barrier surrounding each Pt NP. At 800 °C (Figure 3f), both sintering of Pt NPs and growth of CeO_2 crystallites started to occur, which was manifested by the formation of Pt large agglomerates and a substantial increase in grain size for CeO_2. The X-ray powder diffraction pattern (Supporting Information, Figure S2a) taken from these samples confirmed that the CeO_2 phase remained to be in a cubic fluorite structure. For the product obtained at 800 °C, a weak peak at 39.6 degrees appeared, which could be assigned to the (111) diffraction of Pt, indicating the formation of Pt large agglomerates by sintering. The changes in size for the embedded Pt NPs (measured from the TEM images) and the CeO_2 crystallites (derived from the XRD patterns using the Debye–Scherrer equation) after the samples had been

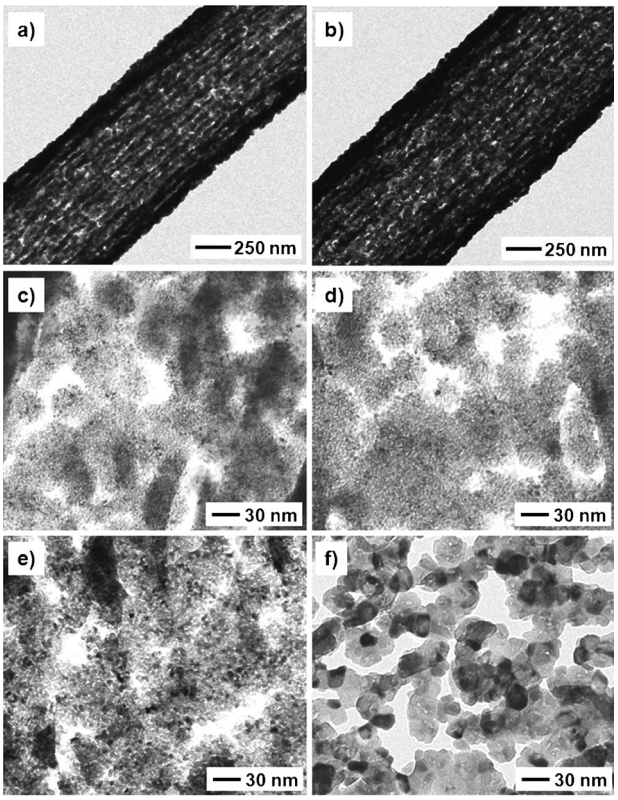

Figure 3. a), b) Low-magnification TEM images showing a Pt_{encap}/CeO_2 hollow fiber after it had been calcined in air for 2 h at a) 400 and b) 800 °C. c)–f) High-magnification TEM images revealing the wall structures of the Pt_{encap}/CeO_2 hollow fibers after calcination in air for 2 h at c) 400, d) 600, e) 700, and f) 800 °C.

treated in air at different temperatures are shown in the Supporting Information, Figure S2b. Up to 400 °C, no significant change in size was observed for both the Pt NPs and CeO_2 crystallites. When the temperature was increased from 400 to 700 °C, the average sizes of the Pt NPs and CeO_2 crystallites were increased from 3.5 to 4.1 nm and from 3.2 to 5.1 nm, respectively. As the temperature was further increased to 800 °C, the Pt NPs grew to 12 nm and the CeO_2 crystallites also grew to 11.2 nm, which is more than triple relative to their original sizes. The missing diffraction peak at 39.6° for Pt for all the samples until 700 °C also suggested that the new Pt_{encap}/CeO_2 system could resist thermal sintering up to this temperature. Above 700 °C, the simultaneous sintering of CeO_2 crystallites may have induced and facilitated sintering of the Pt NPs, leading to a quick increase in size for the Pt NPs. We also tried to resolve possible changes to the morphology of Pt NPs and the platinum–oxide interface by high-resolution TEM (Supporting Information, Figure S3), but it was very difficult to obtain any meaningful data owing to the presence of a polycrystalline CeO_2 matrix around each Pt NP.

We measured the surface areas of the Pt NPs embedded in the Pt_{encap}/CeO_2 hollow fibers by CO titration of chemisorbed oxygen (Supporting Information, Table S1). The titrations were performed at −20 °C to minimize oxygen spillover to Pt sites from CeO_2. For the samples treated at 400, 600, 700, and 800 °C in air for 2 h, the accessible Pt surface areas and the corresponding Pt dispersions were found to be in the ranges of 0–3.4 $m^2 g^{-1}$ and 0–1.7 %, respectively. Unexpectedly, CO titration failed to give a measurable Pt surface area and dispersion for the Pt_{encap}/CeO_2 sample calcined at only 400 °C. It is possible that organic residues from the incomplete combustion of PVP and PS might have blocked the channels in the CeO_2 sheath so that the O_2/CO analytes could not access the surface of Pt NPs. After calcination at 600 °C, which presumably allowed more of the organic residues to be burned away, CO titration gave a Pt surface area of 2.6 $m^2 g^{-1}$ and dispersion of 1.2 %. The highest accessible Pt surface area (3.4 $m^2 g^{-1}$) and dispersion (1.7 %) were obtained after calcination at 700 °C. By further increasing the calcination temperature to 800 °C, the surface area and dispersion dropped to 0.8 $m^2 g^{-1}$ and 0.4 %, respectively, which is consistent with the sintering of Pt NPs observed by TEM and XRD.

Figure 4 compares the TOFs of CO oxidation reaction obtained for two samples of Pt_{encap}/CeO_2 hollow fibers and a Pt/SiO_2 catalyst reported by Cant and co-workers.[21] The Pt/SiO_2 TOFs fit the same Arrhenius curve extrapolated from higher-temperature measurements under the same conditions on clean Pt(100) and clean, well-defined Pt nanoparticles of different sizes supported on planar SiO_2 substrates,[22] and thus represent the expected structurally insensitive activity of normal Pt sites. Also shown are TOFs for a Pt/TiO_2 catalyst prepared in the same way as the structure shown in Figure 2b,[23] with a Pt dispersion of 31 % by CO titration. These TOFs are almost identical to Pt/SiO_2, as expected for the normal metallic Pt sites. The Pt_{encap}/CeO_2 hollow fibers exhibited TOFs three orders of magnitude higher than those of the Pt/SiO_2 and Pt/TiO_2 catalysts within the comparable temperature range of 384–476 K, providing a direct evidence to support its far superior catalytic activity. These TOFs were calculated based on the Pt dispersion measured by CO titration (Supporting Information, Table S1), which were essentially unchanged after these catalytic rate measurements (not shown), but which were about 10-fold less than what was measured from the size of the Pt NPs using TEM. Even considering the worst possible experimental errors in dispersion, the activity of the Pt_{encap}/CeO_2 hollow fibers was still more than 100-fold higher than the Pt/SiO_2 and clean Pt model catalysts. Also, if we used the average particle size of 4.1 nm measured by TEM after calcination at 700 °C to calculate the Pt surface area (assuming no poisoned Pt sites), it gave 40 m^2 of Pt. Based on this area, we still calculate a TOF that was ca. 100-fold higher than that of the Pt/SiO_2. Moreover, it is worth pointing out that the Pt/SiO_2, Pt/Al_2O_3, and $Pt/CeO_X/Al_2O_3$ catalytic systems studied by other groups[24] all exhibited much lower TOFs than that of Pt_{encap}/CeO_2 hollow fibers under the same conditions with O_2/CO_2 ratio = 0.5. In studies of CO oxidation over traditionally prepared Pt/CeO_2 catalysts, it was reported that the CO oxidation activity of Pt, which ended up partially covered and/or encapsulated by a thin layer of CeO_2, was higher than that of Pt itself.[7,25,26] However, those prior studies only showed a 3–4-fold increase in TOF, which is much less than the 1000-fold increase observed here. The CeO_2 layer on Pt was suggested to accelerate the overall reaction rate by participating in accepting and donating oxygen atoms, which compensated the limited accessibility of reactants to the catalytic sites.[27,28] A roughly 100-fold increase in Pt activity owing to CeO_2 was reported when the CO/O_2 ratio was about 1000, which could be attributed to oxygen spillover to the Pt from the CeO_2 if the Pt sites were too saturated by

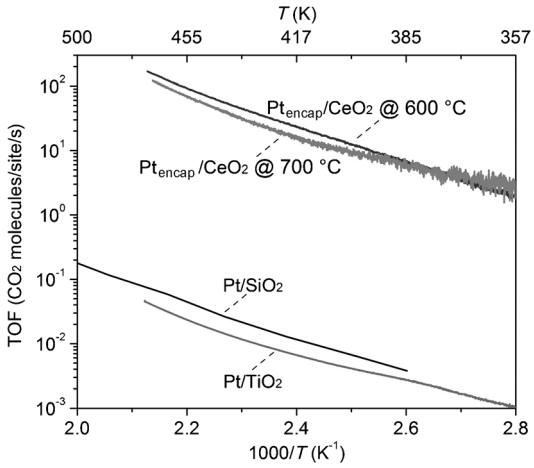

Figure 4. Turnover frequencies (TOFs) at an O_2/CO ratio of 1:2 versus temperature for Pt_{encap}/CeO_2 hollow fibers calcined at 600 and 700 °C for 2 h. For comparison, TOFs are also shown for a conventional Pt/SiO_2 catalyst (5 wt % Pt), as reported by Cant and co-workers[21] under the same reaction conditions. As discussed in the text, this Pt/SiO_2 catalyst had TOFs similar to those of a clean Pt(100) surface. They were also nearly identical to the TOFs obtained for a Pt/TiO_2 catalyst under the same conditions, confirming that the TOFs of the Pt/SiO_2 were as expected for normal metallic Pt sites, and that the new Pt_{encap}/CeO_2 system was 1000-fold faster.

CO to dissociate O_2, but no increase owing to CeO_2 was observed in that study at the stoichiometric ratio used here.[29] For the hollow Pt_{encap}/CeO_2 fibers described here, the CeO_2 nanocrystalline sheath tightly surrounding the Pt NPs with a maximized Pt–CeO_2 interface greatly benefitted the catalytic CO oxidation rate. Further studies on the mechanism of CO oxidation using the Pt_{encap}/CeO_2 system are required to understand this phenomenon.

In summary, we have demonstrated a method for embedding Pt NPs in the inner surfaces of CeO_2 hollow fibers with open ends to generate a new catalytic system that could resist thermal sintering up to 700 °C. The TOF of the as-synthesized Pt_{encap}/CeO_2 hollow fibers for CO oxidation was 2–3 orders of magnitude higher than those based on the conventional Pt/SiO_2 catalytic system, which could be attributed to a unique structure and composition for maximizing the Pt_{encap}/CeO_2 interface. Future work will involve the introduction of a protective layer based on oxides, such as SiO_2 or Al_2O_3, to the Pt_{encap}/CeO_2 catalytic system to achieve high reactivity and sintering resistance at temperatures even higher than 700 °C.

Received: May 15, 2012
Published online: August 29, 2012

Keywords: ceria hollow fibers · electrospinning · platinum nanoparticles · sinter resistance

[1] S. J. Tauster, S. C. Fung, R. L. Garten, *J. Am. Chem. Soc.* **1978**, *100*, 170.
[2] J. Guzman, S. Carrettin, J. C. Fierro-Gonzalez, Y. Hao, B. C. Gates, A. Corma, *Angew. Chem.* **2005**, *117*, 4856; *Angew. Chem. Int. Ed.* **2005**, *44*, 4778.
[3] G. Dutta, U. V. Waghmare, T. Baidya, M. S. Hegde, *Chem. Mater.* **2007**, *19*, 6430.
[4] X.-B. Zhang, J.-M. Yan, S. Han, H. Shioyama, Q. Xu, *J. Am. Chem. Soc.* **2009**, *131*, 2778.
[5] Q. Fu, H. Saltsburg, M. Flytzani-Stephanopoulos, *Science* **2003**, *301*, 935.
[6] D. Tibiletti, A. Goguet, F. C. Meunier, J. P. Breen, R. Burch, *Chem. Commun.* **2004**, 1636.
[7] C. Hardacre, R. M. Ormerod, R. M. Lambert, *J. Phys. Chem.* **1994**, *98*, 10901.
[8] M. Abid, R. Touroude, *Catal. Lett.* **2000**, *69*, 139.
[9] J. Silvestre-Albero, F. Rodríguez-Reinoso, A. Sepúlveda-Escribano, *J. Catal.* **2002**, *210*, 127.
[10] H. C. Yao, Y. F. Yao, *J. Catal.* **1984**, *86*, 254.
[11] E. C. Su, W. G. Rothschild, *J. Catal.* **1986**, *99*, 506.
[12] G. N. Vayssilov, Y. Lykhach, A. Migani, T. Staudt, G. P. Petrova, N. Tsud, T. Skála, A. Bruix, F. Illas, K. C. Prince, V. Matolin, K. M. Neyman, J. Libuda, *Nat. Mater.* **2011**, *10*, 310.
[13] A. Caballero, J. P. Holgado, V. M. Gonzalez-DelaCruz, S. E. Habas, T. Herranz, M. Salmeron, *Chem. Commun.* **2010**, *46*, 1097.
[14] U. Diebold, *Surf. Sci. Rep.* **2003**, *48*, 229.
[15] S. Bernal, J. J. Calvino, M. A. Cauqui, J. M. Gatica, C. Larese, J. A. Pérez Omil, J. M. Pintado, *Catal. Today* **1999**, *50*, 175.
[16] H. P. Zhou, H. S. Wu, J. Shen, A. X. Yin, L. D. Sun, C. H. Yan, *J. Am. Chem. Soc.* **2010**, *132*, 4998.
[17] C. M. Y. Yeung, K. M. K. Yu, Q. J. Fu, D. Thompsett, M. I. Petch, S. C. Tsang, *J. Am. Chem. Soc.* **2005**, *127*, 18010.
[18] C. M. Y. Yeung, S. C. Tsang, *J. Mol. Catal. A* **2010**, *322*, 17.
[19] Y. Dai, B. Lim, Y. Yang, C. M. Cobley, W. Li, E. C. Cho, B. Grayson, P. T. Fanson, C. T. Campbell, Y. Sun, Y. Xia, *Angew. Chem.* **2010**, *122*, 8341; *Angew. Chem. Int. Ed.* **2010**, *49*, 8165.
[20] T. Yu, B. Lim, Y. Xia, *Angew. Chem.* **2010**, *122*, 4586; *Angew. Chem. Int. Ed.* **2010**, *49*, 4484.
[21] N. W. Cant, P. C. Hicks, B. S. Lennon, *J. Catal.* **1978**, *54*, 372.
[22] S. M. McClure, M. Lundwall, Z. Zhou, F. Yang, D. W. Goodman, *Catal. Lett.* **2009**, *133*, 298.
[23] E. Formo, E. Lee, D. Campbell, Y. Xia, *Nano Lett.* **2008**, *8*, 668.
[24] Y. J. Mergler, A. van Aalst, J. van Delft, B. E. Nieuwenhuys, *Appl. Catal. B* **1996**, *10*, 245.
[25] A. M. Contreras, X.-M. Yan, S. Kwon, J. Boker, G. A. Somorjai, *Catal. Lett.* **2006**, *111*, 5.
[26] Y. Suchorski, R. Wrobel, S. Becker, H. Weiss, *J. Phys. Chem. C* **2008**, *112*, 20012.
[27] S. Golunski, R. Rajaram, N. Hodge, G. J. Hutchings, C. J. Kiely, *Catal. Today* **2002**, *72*, 107.
[28] S. Golunski, R. Rajaram, *CATTECH* **2002**, *6*, 30.
[29] T. Bunluesin, E. S. Putna, R. J. Gorte, *Catal. Lett.* **1996**, *41*, 1.

